Journal of Cleaner Production 202 (2018) 109–119

Contents lists available at ScienceDirect

Journal of Cleaner Production

journal homepage: www.elsevier.com/locate/jclepro

Dynamic control strategy in partially-shaded photovoltaic power plants for improving the frequency of the electricity system

Claudia Rahmann [a, *], Carolina Mayol [a], Jannik Haas [b]

[a] Department of Electrical Engineering, University of Chile, Chile
[b] Department of Stochastic Simulation and Safety Research for Hydrosystems (IWS/SC SimTech), University of Stuttgart, Germany

ARTICLE INFO

Article history:
Received 24 May 2018
Received in revised form
25 July 2018
Accepted 30 July 2018
Available online 31 July 2018

Keywords:
Artificial neural networks
Control strategy
Frequency control
Partial shading
Photovoltaic generation
Solar radiation forecasting

ABSTRACT

When large-scale photovoltaic power plants (PV-PPs) operate under partially-shaded conditions, their power output can be extremely fluctuating. This situation may compromise the energy balance of the electricity grid, which in turn threatens its secure operation from a frequency control viewpoint. In this context, the development of control strategies to reduce the variability of the power generated by PV-PPs is a key issue towards reaching sustainable electric systems. With this purpose, this paper proposes a novel control strategy to reduce the negative effects that PV-PPs operating under partially-shaded conditions may cause on the frequency control of electricity grids. The control operates the PV-PP in deload mode, i.e. keeping power reserves. The deload level of the PV-PP is set dynamically during the day considering a 10-min forecast of solar generation. The forecast is performed with artificial neural networks, first predicting the day-type (sunny, cloudy, overcast) and then the solar power. The controller continuously monitors the condition of the PV-PP: when the plant is under non-uniform shaded conditions, it deploys the power reserves to smooth the PV power. The proposed control was applied to a Chilean case study focused on the Atacama Desert, testing different control rules for the deload level. The obtained results show that the implementation of the proposed control considerably improves the frequency performance of the electricity grid. Although operating in deload mode implies energy losses in the PV-PP, the use of a dynamic deload level minimizes these losses when compared to a constant deload level. Altogether, the dynamic simulations show that such a control can play a relevant role for frequency control in electrical power systems with high shares of photovoltaic power. Our findings give important insights to electricity regulators about the technical requirements that they should impose to large-scale PV-PPs in electric power systems dominated by renewables energies.

1. Introduction

The deployment of large-scale photovoltaic power plants (PV-PPs) has been remarkable during the last years. The worldwide installed capacity of PV generation exceeded 300 GW in 2016 with a yearly growth rate of 70 GW (REN21, 2017). Chile contributed with an installed capacity of around 2 GW. Towards a more sustainable society, the penetration of solar power plants, together with other renewables technologies (Hašková, 2017; Mardoyan and Braun, 2015), will need to keep on growing. Chile is particularly interesting given its relevance in the worldwide copper market, an essential material for renewable technologies. Higher shares of renewable generation would consequently also imply a cleaner copper production (McLellan et al., 2012; Moreno-Leiva et al., 2017).

However, large shares of renewable generation technologies may significantly affect the operation of electric power systems (Carvalho et al., 2011; Jones, 2017). For a satisfactory operation of the electricity grid, the frequency should remain nearly constant around its nominal value (50 Hz in Europe). This means that at each point in time, electric power systems must keep the total energy production equal to the total consumption. In case of a generation surplus, the grid frequency increases; for generation deficits, the opposite happens. This balance management is called frequency control or frequency regulation. An energy imbalance can trigger the disconnection of key system components, which in turn may lead to a system blackout. Accordingly, frequency control represents a vital task for ensuring the security of the electricity supply.

* Corresponding author.
E-mail address: crahmann@ing.uchile.cl (C. Rahmann).

https://doi.org/10.1016/j.jclepro.2018.07.310
0959-6526/

The variability and uncertainty of solar power impose different challenges to transmission system operators (TSOs) (Faranda and Leva, 2008), especially regarding the frequency regulation of the electricity grid (Eto et al., 2010); (Ruiz-Rodriguez et al., 2016). The variability of solar energy occurs on different time scales. On the one hand, under a clear sky, the daily solar resource follows the typical "hill-shaped" profile, which changes with the seasons in response to the sun-earth geometry. On the other hand, passing clouds provoke short-term (seconds to minutes) fluctuations often called cloud-transients (Kankiewicz et al., 2010). As PV-PPs usually operate at their maximum power point (MPP), these irradiance fluctuations are directly converted into power variations. In California, for instance, large-scale PV-PPs have shown power changes over 70% in a 5–10 min timeframe during partially clouded days (Mills and Wiser, 2011). These fluctuations are not only large but also difficult to forecast. Moreover, a highly variable net load leads to more intense cycling of conventional power plants, thus directly affecting their operation and maintenance as well as life expectancy (Lew et al., 2013). Beyond a more fluctuating output, partial shading has further negative effects such as a lower power output (difficulty of tracking the maximum power point) (El-Dein et al., 2011; Rani et al., 2013) and hot spots in the PV panels (which may harm the modules) (Bidram et al., 2012; El-Dein et al., 2011). More details on partially-shaded PV installations can be found in the literature, for example in references (Ishaque et al., 2012; Kok Soon Tey and Mekhilef, 2014; Mäki and Valkealahti, 2012).

The intensity and duration of the cloud-transients depend on the PV-PP size, cloud speed, cloud height, and other factors (Hoff and Perez, 2010; Mills et al., 2010; Remund et al., 2015). The issue becomes increasingly more relevant given the numerous large-scale PV-PPs that are being deployed worldwide. In fact, utility-scale PV systems are responsible for the largest capacity additions, a trend that is increasing (SolarPower Europe, 2017). In Chile, this situation is extreme: about 99% of the country's PV installed capacity correspond to large-scale PV-PPs (Haas et al., 2018). The 90% largest plants have an average installed capacity of 70 MW (National Energy Commission of Chile (CNE), 2017). At roughly three hectares per MW, this means areas of 1.5 km by 1.5 km approximately per PV-PP. At these scales, it is frequent to have partial shadowing on some sections of the PV-PP. Naturally, the shadowed areas depend on the cloud size and speed, which may vary widely. Reference (Lave and Kleissl, 2013) addresses the impact of cloud speeds on solar variability. It explored clouds ranging from 0.1 to 3.0 km traveling between 1 and 25 m/s. For example, a 0.5 km-cloud traveling at 5 m/s would shadow one-ninth of an average (70 MW) PV-PP and take about five minutes to cross the whole array.

Considering these challenges, sustainable electric power systems with high levels of solar power can only be achieved by means of innovations and new services able to ensure the secure operation of the electricity grid. Particularly, novel control strategies are needed to allow PV-PPs to contribute actively to regulate the frequency. These strategies may be either the integration of energy storage systems (Cebulla et al., 2018), e.g. batteries (Pamparana et al., 2017) or hydrogen (Bhandari et al., 2014), or PV-PPs operated below their maximum power point.

As what refers to studies about the use of storage technologies for large-scale PV installations, earlier studies (Guishi Wang et al., 2012) propose to smooth the output power of a PV-PP with the help of a redox-flow battery or hydropower plants (with storage capacity) (Jurasz and Ciapała, 2017). Reference (Beltran et al., 2013) generalizes the sizing of storage to provide a constant PV output and found that values around 1 MWh of storage per MW peak of PV are adequate. Controlling a combined PV and storage -under forecast errors- to minimize the resulting variations (ramp-rates) is done in reference (Duchaud et al., 2018). Using batteries to improve system security (real and reactive power for frequency and voltage support) in distributed systems has also been explored (Hill et al., 2012). Many of the ideas above are combined in reference (Hernández et al., 2017). They study the how frequency can be improved (primary frequency control and inertial response) with a PV unit supported by a hybrid energy storage, including its sizing, and conclude that this system can effectively do the job. For very quick variations of solar radiation, capacitors are also an option for controlling the power fluctuations of PV-PPs (Kakimoto et al., 2009). Other alternatives for mitigating PV power fluctuations, such as flywheels, ultracapacitors, and fuel cells are presented in reference (Shivashankar et al., 2016). Production of hydrogen could also become economically viable soon to use energy excesses of solar generation (Maroušek et al., 2013). Although energy storage systems are an adequate technical alternative, their use for mitigating power fluctuations still involves high investment costs, which may discourage their use depending on the market conditions.

Research about mitigating the variability of the power generated by PV-PPs without the use of storage technologies still remains sparse. Reference (Craciun et al., 2013) is one of the few examples; it operates the PV-PP below its MPP, leaving ramp-up capacity for frequency support and the ability to limit the fluctuations of the power output of the PV-PP. The work presented in (Xin et al., 2013) proposes a strategy (droop control) in PV-PPs for primary frequency support, including an additional emergency control that allows reducing the PV power to avoid large frequency deviations during severe disturbances. The decentralized structure allows the control to be applied to large-scale PV-PPs. For electrical power distribution, the authors of reference (Yang et al., 2014) present a control strategy for keeping a constant PV output power when a power or voltage limit of the grid is reached. The power difference to the MPP is curtailed. In their case study, they calculated that limiting the output power to 80% (of the possible output) implies losing about 6% of energy per year. In our previous work, we proposed a strategy based on sectioning the PV-PP in different zones, in which each zone keeps a given level of reserve achieved by means of deloaded operation (Rahmann et al., 2016). If one or more zones are (partially) shaded, the control deploys the reserves of the unshaded areas. This action allows smoothing power plant's output. Although the proposed strategy showed a good performance from a technical viewpoint, the deload level (and thus the reserve margin of the PV-PP) was kept constant during the whole day, thus making it economically less attractive. The main hypothesis of the present work is that a dynamic deload level (set dynamically during the day) can achieve a good technical and economic performance given an accurate forecast of the solar irradiation.

The present work proposes a dynamic control strategy to reduce the negative effects that large-scale PV-PPs operating under partially-shaded conditions may cause in the frequency regulation of the electricity grid. The control dynamically sets a reserve level over time, considering a 10-min ahead forecast of the solar irradiation and system operating conditions. The forecast is done based on a set of artificial neural networks distinguishing the kind of day in terms of variability of the solar radiation. The control is designed to allow PV-PPs to participate in the frequency regulation while minimizing the energy curtailment. Innovative controls such as the proposed here represent the basis to design new services to be provided by PV-PPs in the future. Indeed, in electric power systems with large shares of solar generation, this kind of functions will be technically needed, and thus they should be remunerated as

ancillary service.

The next section briefly reviews the existing literature for solar forecasting. Section 3 summarizes the proposed control strategy including the controller and forecast model. Section 4 describes the case study. Finally, the results are presented in Section 5 and the conclusions in Section 6.

2. Review: solar forecasting methods

There are many methods for PV-forecasting. Their accuracy strongly depends on the involved temporal and spatial scale. Regarding the temporal scale, for short-term forecasting (minutes to a couple of hours), statistical methods are frequently chosen (Diagne et al., 2013; Huang et al., 2013). Short-term forecasts between 0.5 and 6 h are usually addressed with ground-based or satellite images to determine the cloud motion (Diagne et al., 2013; Rigollier et al., 2004). Long-term forecasting, i.e. from 6 h to days, is often performed with numerical weather predictions (Diagne et al., 2013). Regarding the spatial scale, the challenge of forecasting the production of a small PV system usually lies in the high variability of the local weather. In the case of large-scale PV-PPs, although the spatial distribution of the panels smoothens out part of their fluctuations, the forecast needs to deal with multiple external variables such as humidity, irradiance, and temperature from different weather stations (Zhang et al., 2014). Hence, in practice, the forecast types are frequently grouped according to the PV-system size: small-distributed PV arrays (Bacher et al., 2009; Shi et al., 2012), large centralized PV-PPs (Mao et al., 2013) or aggregated PV production at system level (Zhang et al., 2014).

Among the most used methods to forecast solar irradiance and/or output power of PV-PPs in short time-frames are *autoregressive methods* (for instance, Autoregressive Moving Average –ARMA- (Diagne et al., 2013) and Autoregressive Integrated Moving Average –ARIMA- (Reikard, 2009)), *statistical time series analysis* (Markov chains (Ngoko et al., 2014)), and *artificial neural networks* (Inman et al., 2013; Voyant et al., 2017). Other less used approaches are cloud imagery (Chow et al., 2011), unobserved components models (Harvey, 1990), transfer functions (Reikard, 2009), among others. For a detailed overview of existing forecast methods, references (Diagne et al., 2013; Inman et al., 2013; Voyant et al., 2017) can be consulted.

The upside of autoregressive linear methods is that they are easy-to-implement and accurate (Reikard, 2009). The downside is that they demand a large amount of data and are able to model linear effects only (Box et al., 2015). On the other hand, as traditional time series analysis requires the data to be stationary, some work must be done to capture seasonality and the stochastic nature of the irradiance. If enough data is available, these methods can accurately forecast the irradiance. However, the analysis requires intensive computational processing.

Reference (Inman et al., 2013) reviewed over 200 publications on solar forecasting methods and confirms the successful use of artificial neural networks (ANN) from the subhourly to the yearly timeframe in both data poor and data-rich applications. Another study follows a similar structure by looking at 100 publications and underlines the flexibility of ANN (Voyant et al., 2017). Based on the available data and conducted review, we have decided to apply ANN, which have been proven to be an efficient forecasting technique.

ANN are models inspired by human neurons. They learn based on data by building an input-output mapping. Key advantages of ANN are that they do not require deriving the equations of the model explicitly and can capture nonlinear behaviors for the system under study.

An ANN consists of many interconnected neurons, organized by layers. Each connection (between two neurons) has a weight (Rehman and Mohandes, 2008), which is adjusted in the learning process. In the simulation, each neuron (i) receives a signal (x_{ij}) from the neurons of the previous layer. Each neuron proceeds to add up all its received signals multiplied by the weights of the corresponding connection. From that sum, each neuron then subtracts a fixed value called the activation threshold or bias (w_{i0}), attaining the internal activity level (a_i). This threshold makes sure that only values above it generate a meaningful neuron output (y_i), once the activation function (ϕ) of Equation (2) is applied. (The goal of ϕ, a nonlinear function, is to squeeze the neurons activity -a real number-into a range between 0 and 1. Here, very negative numbers adopt values close to zero, whereas very positive numbers are close to one). The resulting neuron output is then passed on to the next layer.

$$a_i = \sum_{j=1}^{n} w_{ij} \cdot x_{ij} - w_{i0} \tag{1}$$

$$y_i = \phi(a_i) \tag{2}$$

The ability of ANN easily capturing nonlinear effects and their proven accuracy in short timeframes are their main advantages for forecasting solar irradiance or PV output power (Chen et al., 2011; Rehman and Mohandes, 2008). However, if the long-term system conditions change (e.g. climate change), they would need to be updated.

3. Dynamic control strategy

In this section, we detail the methods of our study. We propose a dynamic control strategy composed of a forecasting model and a controller. The strategy is based on solar panels operating in deload mode in order to keep some power reserves. The level of deload is set dynamically over time considering a 10-min solar irradiation forecast and the operating conditions of the electricity grid.

To implement the proposed control, the PV-PP must allow tracking of multiple maximum power points. This can be achieved by different inverter architectures, including string, multi-string, and central inverters (Bidram et al., 2012; Kouro et al., 2015). In these configurations, the PV-PP can be seen as divided into different sections (strings or sets of strings), each of them composed by several panels connected to the network either through DC/AC converters or through DC/DC inverters (which are then connected to a central DC/AC inverter). These types of configurations are widely used in large-scale grid-connected PV systems (Kouro et al., 2015; Li and Wolfs, 2008).

A general block diagram of the control strategy is shown in Fig. 1. It is composed by two main blocks: “Forecasting model” and “Controller”. The forecasting model is in charge of predicting the PV generation 10-min ahead $(\tilde{P}_{out_{t+10}})$ based on a set of ANN. The controller is composed by the blocks “Deload level”, “Supervisory control”, and several “Local control *i*”. While the supervisory control acts over the whole PV-PP (from a centralized perspective), the local controls act locally in each section of the PV-PP.

3.1. Forecasting model

Contrasted to sunny or overcast days, forecasting the solar irradiation in partially clouded conditions is particularly challenging. Different studies have shown that considering the type of day (sunny, cloudy, and overcast) results in more precise forecasts, as when only using one model for a generic kind of day (Ahrens, 2012). Further, due to the many stochastic drivers involved, the

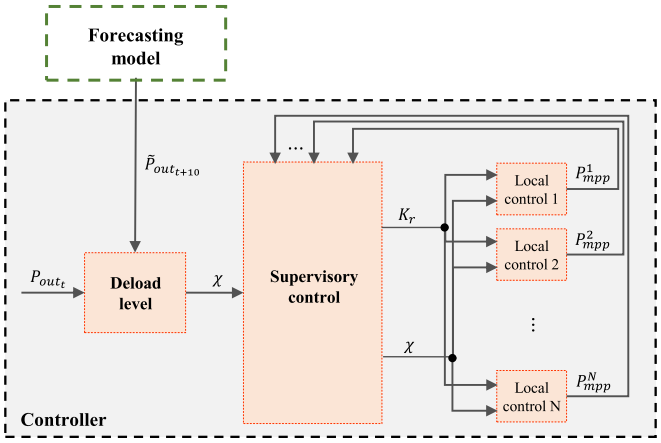

Fig. 1. Block diagram of the dynamic control strategy.

accuracy of forecasts quickly declines with the prediction horizon (Pelland et al., 2013). Based on this background (and the learnings from Section 2), our forecast model for the irradiance consists of two main stages (see Fig. 2):

Stage one: an ANN forecasts the day-type (overcast, sunny, cloudy) of tomorrow ($d+1$). The classification of these days is based on the clear-sky index (CSI) (Larrañeta et al., 2015) as presented in Table 1. This ANN has three inputs from the day before: day-type (CSI_d), average temperature ($\overline{T}_d$), and average global solar radiation ($\overline{GSR}_d$). See the left part of Fig. 2.
Stage two: three ANNs (one for each day-type) are in charge of forecasting the solar radiation 10-min ahead, as shown in the right part of Fig. 2.

In the construction of the ANNs, a correlation analysis was performed using the Spearman correlation coefficient since it captures the monotonic relationship between the random and the other variables (Papaefthymiou et al., 2006). Concretely, for the first stage (CSI-ANN), the clear-sky index of the next day (CSI_{d+1}) is correlated with the corresponding day of the year ($d+1$), and with other variables of the day d (e.g. average temperature, average global solar radiation, average relative humidity, clear sky index). For the ANNs specific to each day-type, the global solar radiation of the next ten minutes (GSR_{t+10}) was correlated with the current values of global solar radiation, relative humidity, and temperature, as well as with the current day of the year (d). These variables were

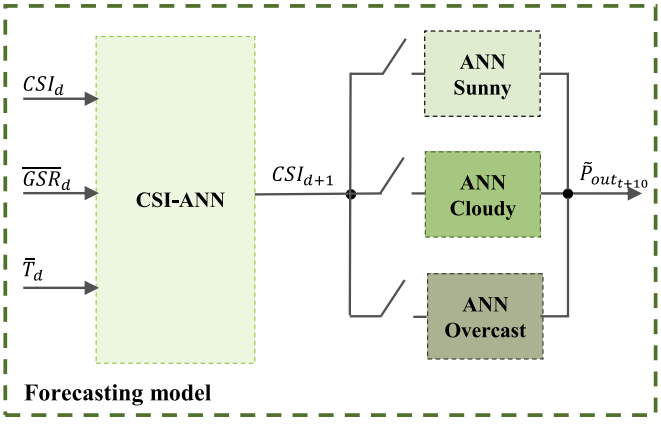

Fig. 2. General block diagram of the forecasting model.

selected because of the availability of real data. The activation functions used in all ANN were Sigmoid.

Regarding the input data division for training, validation, and testing of the ANNs:

- The input data for the CSI-ANN are first categorized into types of day and then separated into the different kinds of days to avoid over-representation of one type of day in either of the subsets and to ensure each type of day was well represented. The data was finally divided in order to have the subsets for training, validation, and testing with a proportion of 70-20-10%.
- The sets for each GSR-ANN are selected such that the 10-min daily data was not broken apart for different training sets. This means that each 10-min data was used in the same set (training, validation, and test) that the rest 10-min data of the same day. The data was then divided into training, validation, and testing subsets in a proportion of 70-20-10%, respectively. However, in this case, a 10-fold cross-validation process was set in order to avoid overfitting of the network and to have a better generalization capability in the final model.

Each fold ANN was then compared with each other, and there were no statistically significant differences among them, which confirms that the sets were statistical homogenous. The number of nodes in the hidden layer of the ANNs is determined by trial-and-error, which is a common practice in this kind of forecasts (Liu et al., 2015).

3.2. Controller

As shown in Fig. 1, the "Controller" is composed by the blocks "Deload level", "Supervisory control", and several "Local control i". The block "Deload level" uses the forecasted PV power ($\tilde{P}_{out_{t+10}}$) and the current PV generation (P_{out_t}) to set the deload level (χ) at which the panels of each section should operate. Since the objective is to mitigate the variability of the power generated by the PV-PP, the deload level is defined considering the (forecasted) variation of the PV output power over a period of 10 min, i.e.:

$$\chi = f\left(\tilde{P}_{out_{t+10}}, P_{out_t}\right) \tag{3}$$

The block "Supervisory control" constantly monitors each section of the PV-PP through the signal P^i_{mpp}. When shadows are cast on one or more sections of the PV-PP, the supervisory control orders to deploy some power reserves in order to counteract the power deficit. Considering a deload level (χ) ranging from 0 to 1, the amount of operating reserves available in the PV-PP is calculated based on:

$$R_t(\chi) = \sum_{i=1}^{N} P^i_{mpp}(H,T)\cdot\chi \tag{4}$$

where P^i_{mpp} is the maximum power of section i (as a function of temperature T and irradiance H), and N the amount of sections in the PV-PP. The ideal operating condition is that each section of the PV-PP receives the same irradiation level. If that is not the case, the power deficit ΔP due to the shading situation is calculated according to:

$$\Delta P = \left\{ \sum_{i=1}^{N} max\left\{P^i_{mpp}\right\}_{i=1\ldots N} - P^i_{mpp} \right\}\cdot(1-\chi) \tag{5}$$

In other words, ΔP is greater than zero only when at least one PV

section is operating with a solar irradiation level different from the rest. Otherwise, ΔP becomes zero, and hence, no action is taken.

The supervisory control regulates the deployment of the power reserves through the signal K_r. This signal is calculated based on the operating reserves R_t and the power deficit ΔP according to:

$$K_r = \begin{cases} 1 - \dfrac{\Delta P}{R_t(\chi)} & 0 \le \Delta P \le R(\chi) \\ 0 & \Delta P > R(\chi) \end{cases} \quad (6)$$

From Eq. (6) it can be seen that the signal K_r takes values between $[0, 1]$. When $K_r = 1$ ($\Delta P = 0$), no action is taken and each, PV section maintains its current operation. On the other hand, when $K_r < 1$, the power reserves are deployed in order to smooth the output power of the whole PV-PP.

Each PV section receives and reacts on the control signal K_r by changing (or sustaining) its output power accordingly. The local controls implemented at each section i, use a $d-q$ reference frame. The deloading technique used for allowing the sections to keep some power reserves is achieved by decreasing the PV voltage below the MPP voltage (Rahmann et al., 2016).

4. Case study

4.1. Electric power system under study and data

The isolated Northern Interconnected System (NIS) of Chile is studied here. Its generation matrix is based on fossil fuels generation (coal, oil and natural gas). The projected peak load for 2020 is 3300 MW, characterized by about 90% of industrial and 10% of residential load (National Energy Commission of Chile (CNE), 2016). At the time of this study, the NIS was still operating in isolated mode, separated from the rest of the country. The islanding operation, together with slow generation units with limited ramp rates and low levels of inertia, has led the NIS to constantly have a poor frequency regulation performance.

Placed in the heart of the Atacama Desert, the system has access to one of the highest solar potentials around the world (Cordero et al., 2016; Solargis s.r.o., 2018). Accordingly, many large-scale PV-PPs have been deployed during the last years. The scenario under study assumes that about 15% of the system's installed capacity corresponds to PV-PPs (Haas et al., 2018). This corresponds to around 900 MW of the total installed capacity of the system by 2020 distributed among fourteen PV-PP. The PV-PPs are allocated in three zones throughout the system. The structure of the electricity grid, the location of the meteorological stations, and the location of the PV-PPs are shown in Fig. 3.

In this study, each PV-PP is considered to have multiple maximum power point trackers (such as it is the case of multi-string inverter architectures or central inverters). The PV-PPs were divided into 4 sections, each with its own MPPT and different forecast. The required data for the forecasting model is collected from existing meteorological stations distributed throughout the system (Cordero et al., 2016; Department of Geophysics - University of Chile and Ministry of Energy of Chile, 2012). The ANNs of each zone are trained, validated, and tested with the data from the nearest meteorological station (see Table 2): *PALM*, *CRUC 1,2*, *SLAR* for zones 1, 2, and 3, respectively. These stations include data for radiation (diffuse, direct normal, global horizontal), temperature, humidity, and wind speed, and have a resolution of 10-min.

For the ANNs specific to each day-type, the 10-min data was split into the different day-types, following the classification mentioned earlier (based on the CSI). Table 3 shows the resulting data entries of each station for each day-type. Each of these groups

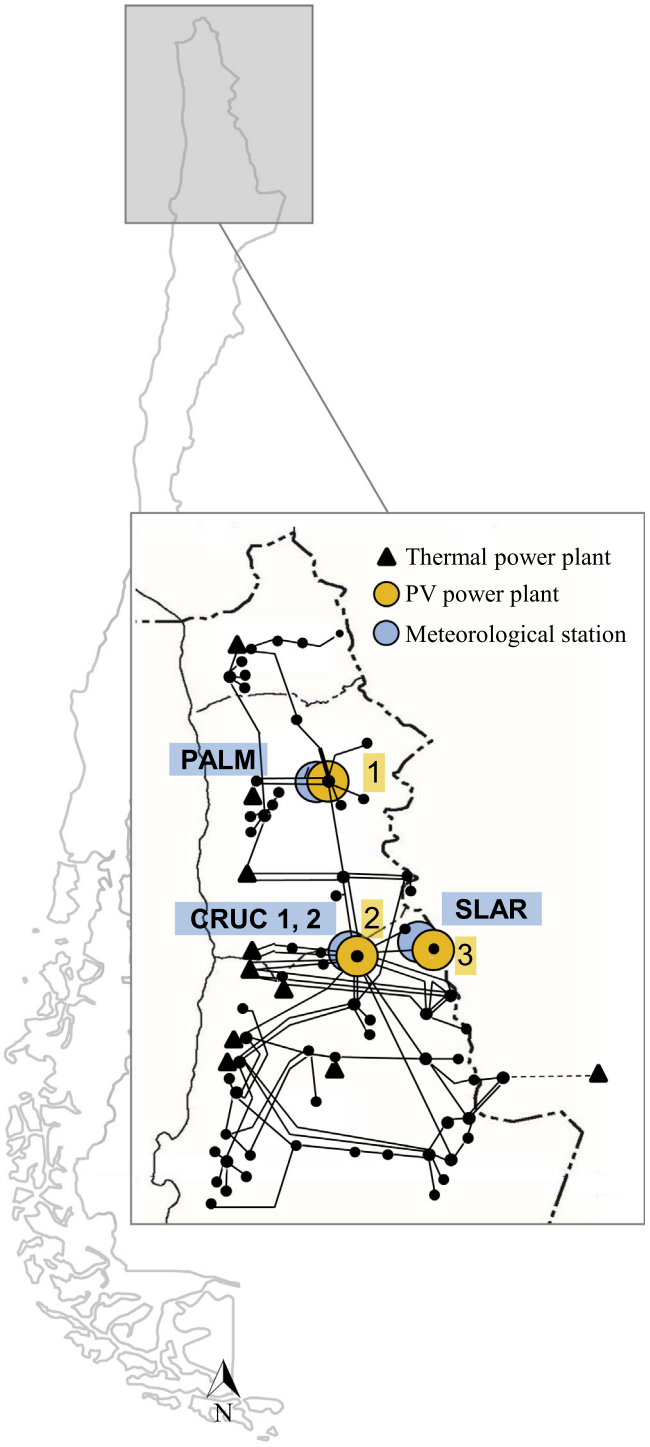

Fig. 3. Simplified diagram of the power system including PV-PPs and meteorological stations.

was used to train the respective ANN. It can be seen that the data availability of SLAR is lower, which could be an issue for the precision of the corresponding ANN.

4.2. Cases considered in the dynamic simulations

The control's dynamic performance was tested on a dynamic model of the NIS (considering its projection to the year 2020). The

Table 1
Classification and description of the types of day according to CSI.

Type of day	Description	CSI
Sunny	Mostly or totally clear day. No clouds.	(0.6 – 1.0]
Cloudy	Mostly covered day with great fluctuations or thin clouds with fluctuations.	(0.3 – 0.6]
Overcast	Totally covered and mostly covered days with some fluctuations.	[0–0.3]

Table 2
Characteristics of the meteorological stations.

	PALM	CRUC 1, 2	SLAR
Latitude	20°15′25″ S	22°16′29″ S	22°20′27″ S
Longitude	69°46′30″ W	69°33′58″ W	68°52′36″ W
Elevation	1024 m.a.s.l.[a]	1185 m.a.s.l.	2526 m.a.s.l.
Data	08/01/2008–10/29/2015	08/28/2009 – 11/11/2014	05/20/2010 – 12/31/2012

[a] m.a.s.l = meters above sea level.

Table 3
Total 10-min data (in thousands) per day-type in each meteorological station.

Station	Sunny	Cloudy	Overcast
PALM	49 k	94 k	41 k
CRUC	45 k	69 k	28 k
SLAR	19 k	22 k	11 k

model of the electric power system was implemented in the simulation tool DIgSILENT Power Factory. The performance of the control strategy (including the forecasting model) was tried out on critical days. These days were selected in terms of the (high) fluctuations of solar radiation. The dynamic simulations were performed considering four different strategies regarding the deload level χ:

- Strategy *S0c*: the control strategy is disabled (0% deload level).
- Strategy *S*15*c*: as in (Rahmann et al., 2016), the control strategy is operated with a constant deload level of 15% during the whole day.
- Strategy S_{Ramp}: the control strategy considers a deload level based on a ramp function.
- Strategy S_{Step}: the control strategy considers a deload level based on a step function.

The deload rules (or strategies) used in this work, S_{Ramp} and S_{step}, are shown in Fig. 4. Here, for example, the point (5%; 5%) indicates that if a power ramp of 5% is forecasted, a deload level of 5% is considered by the controller for the next 10 min. The power ramp is calculated considering the current output power of the PV-PP in time t and the forecasted output power in time $t+10$. For both strategies, we used a minimum deload level of 2% (based on the errors inherent to the forecasting tool), and a maximum level of 15% (based on the best-case reported by (Rahmann et al., 2016)). Other rules could also be considered depending on the power system under study and the characteristics of the solar resource in the location of the PV-PP.

4.3. Data availability

To ensure the use and reproducibility of the proposed control and also to make it easier for readers to extend our work, we have made the data used available in our institutional site (Centro de Energía - University of Chile, 2018). The repository includes the data for the meteorological stations (CRUC, PALM, and SLAR) and the database developed for the NIS in DIgSILENT Power Factory.

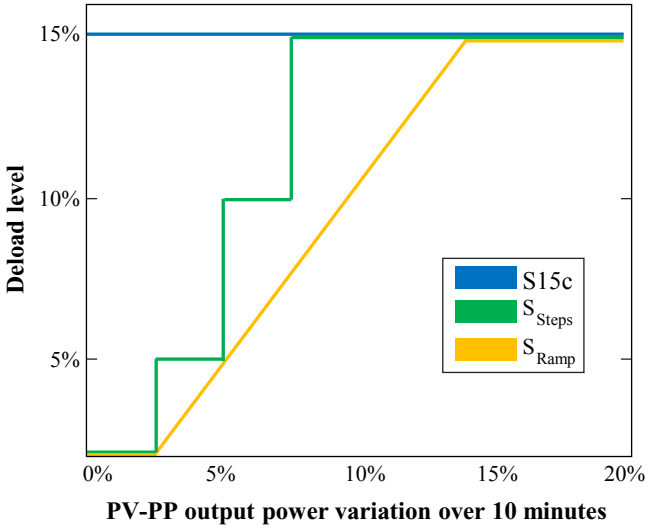

Fig. 4. Considered deload strategies.

Each tab contains the global solar radiation (GSR), relative humidity (RH), temperature (T), day of the year (DOY), month, hour, and minutes plus the type of day calculated.

5. Results and discussion

5.1. Forecasting model

For each zone presented in Fig. 3, four ANNs were trained in order to forecast the generated power by the pertinent PV-PP: one CSI-ANN to forecast the kind of day and three ANNs for each kind of day. The ANN models were created by using Matlab Simulink.

Table 4 presents the number of nodes in the hidden layers and the normalized mean squared error (NMSE) for the CSI-ANNs. It can be seen that the obtained CSI-ANNs present a NMSE between 1.8% and 2.4%.

Fig. 5 illustrates the structure of the obtained ANNs for cloudy and sunny days in the meteorological station PALM. The output of each ANN is the forecasted global solar radiation at time $t+10$.

Since the CSI-ANN can be mistaken, the ANNs of each kind of day are evaluated not only considering the pertinent day, but also the other kinds of days. The results are summarized in Table 5. The ANNs, when evaluated in their corresponding day-type, present an NMSE below 3%. This shows that the forecasting tool has a good

Table 4
NMSE and nodes in the hidden layer per CSI-ANN.

Meteorological Station	Number of nodes in the hidden layer	NMSE of the CSI-ANN
PALM	6	2.4%
CRUC	14	1.8%
SLAR	13	1.9%

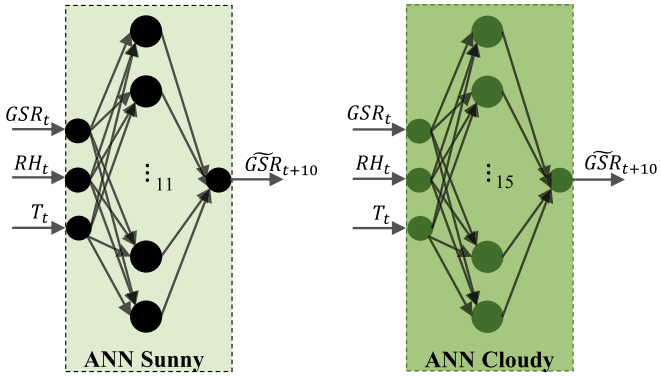

Fig. 5. ANNs for a sunny and cloudy day in the meteorological station PALM.

Table 5
NMSE per ANN for every type of day.

Station	Data	ANN		
		Overcast	Cloudy	Sunny
PALM	Overcast	2.0%	1.9%	2.7%
	Cloudy	4.5%	1.7%	1.2%
	Sunny	4.7%	1.8%	1.3%
CRUC	Overcast	2.3%	3.5%	5.9%
	Cloudy	8.3%	2.9%	2.2%
	Sunny	7.9%	2.9%	1.9%
SLAR	Overcast	3.0%	5.0%	21.1%
	Cloudy	8.6%	2.6%	44.0%
	Sunny	9.7%	2.8%	2.0%

performance when the day-type is correctly predicted. Conversely, when the forecast of the day-type is mistaken, the NMSE increases (to 4.7%, 8.3%, and 44.0% for PALM, CRUC, and SLAR). The imprecision of forecasts in SLAR can be explained by the lack of long-term data, which was already mentioned in Section 4 (see Table 3). Moreover, station SLAR is located within the Atacama Desert, which is characterized by special weather conditions during one month each year. This natural phenomenon, the *Bolivian Winter,* occurs each January and is characterized by increased rainfall in the area. This implies some days in January with unstable weather conditions. The presence of this phenomenon makes it even more imperative to have a larger amount of data in order to achieve good forecasting performance even during extreme conditions.

Fig. 6 presents the forecasted and the measured radiation in the meteorological stations PALM, CRUC and SLAR for the worst-case scenarios in terms of radiation ramps and bias in each of the three stations. Even for these critical cases, the forecasting models perform quite good for all stations. The maximum bias for the sunny day in PALM station is nearly 450 W/m^2 (around 9:00 a.m.). For the cloudy day in CRUC station the peak is around 550 W/m^2 (at 3:30 p.m.), and for the cloudy day in SLAR station it is nearly 430 W/m^2 (around 8:30 a.m.).

5.2. Dynamic performance of the power system

The control's dynamic performance was tested on a dynamic model of the NIS (considering its projection to the year 2020). The model of the system was implemented in the simulation tool DIgSILENT Power Factory. Although the proposed control was tested considering several days of the year, we only present the results for a sunny (Jan. 27, 2014) and a cloudy day (Feb. 11, 2011). These days were selected because they exhibit high solar irradiance variability, meaning that they represent a worst case from a system frequency perspective.

Fig. 7 shows the evolution of the frequency during the day in all considered strategies. The horizontal lines in 49.8 and 50.2 Hz highlight the minimum and maximum values allowed for the frequency during normal operation according to the Chilean grid code (National Commission of Energy, 2016). It can be observed that the implementation of the control always improves the frequency regulation when compared to the case without control (S0c). This is valid for a constant deload level during the day ($S15c$) and dynamic deload levels strategies (S_{Ramp} and S_{Step}). During a cloudy day (Fig. 7a), the control is able to keep the system frequency within the allowable band during the day. However, for a sunny day (Fig. 7b), the frequency drops below 49.8 Hz even when the control is active. Nonetheless, the minimum frequency achieved during the day (49.5 Hz at 17.20 p.m.) is higher than when the control is not used. Moreover, the control strategy decreases the percentage of the time that the frequency is below 49.8 Hz from 30% to 14%, thus significantly improving the frequency regulation. This performance of the control during a critical sunny day could be expected due to the characteristics of the conventional generation units and the isolated nature of the power system. However, the performance could be further enhanced by defining different deload strategies per

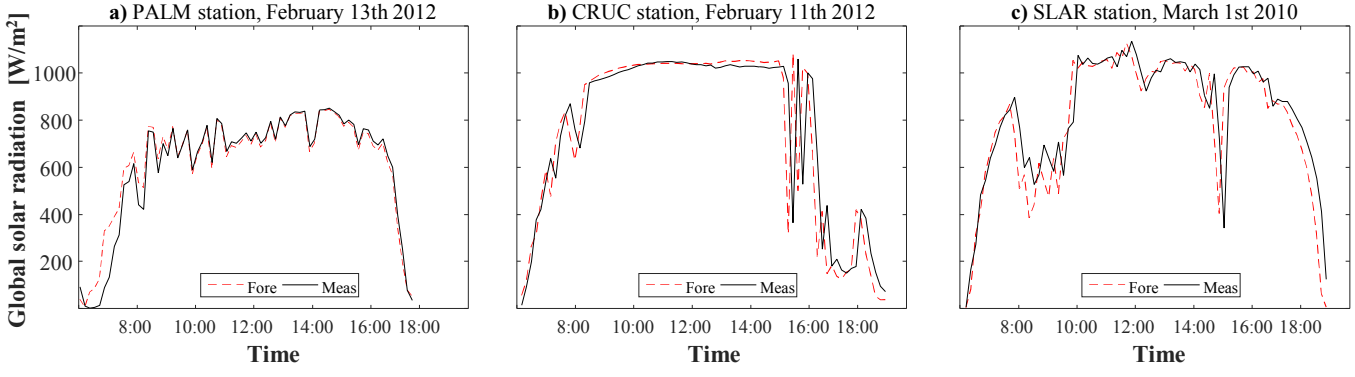

Fig. 6. Results of the forecasting model for all meteorological stations. (a) sunny day, (b) cloudy day, (c) cloudy day.

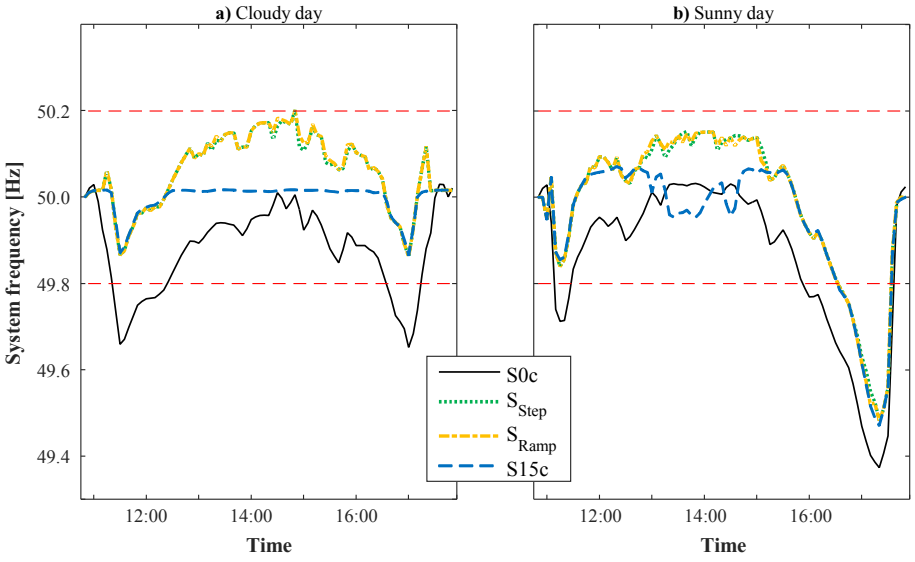

Fig. 7. Frequency for the control strategies $S0c$, $S15c$, S_{Ramp} and S_{Step}. a) Cloudy day and b) sunny day.

type of day.

Fig. 8 shows the energy losses for the strategies $S15c$, S_{Ramp}, and S_{Step}. It can be seen that there is an important difference between considering a constant deload level during the day and a variable one. The energy losses during a cloudy day in case of $S15c$ are around 7%, whereas in the cases S_{Ramp} and S_{Step} are around 2%. Moreover, during a sunny day, the energy losses considering a dynamic deload level are even smaller than 2%. Thus, the definition of a dynamic deload level allows an important reduction of the energy losses of the PV-PP. Moreover, this reduction of energy losses is accomplished without worsening the controller's performance (recalling Fig. 7). It is important to highlight that the energy losses shown in Fig. 8 were calculated for two critical days from a system frequency perspective (i.e. days with high solar irradiance variability). Since our control strategy is designed to more keep power reserves in those days in which the expected variability is high, it can be concluded that the energy losses in other less critical days of the year should be less (or equal) than 2%. Accordingly, we expect that our control strategy loses no more than 2% of solar energy per year.

Fig. 9 shows the changes in the main control signal (K_r) which is in charge of deploying the reserves and changing the deload level in each PV section. During a cloudy day, the control signal K_r of $S15c$ changes more frequently its reference as when compared to the cases S_{Ramp} and S_{Step}. The response when considering the strategies S_{Ramp} and S_{Step} is better from a controller perspective, since less efforts are required. On the contrary, during a sunny day, maximum reserves are deployed more often ($K_r = 0$), because the radiation drops can be more pronounced than during a cloudy day. From this figure, it can also be concluded that a ramp-strategy for the deload level is more efficient than a step-strategy since K_r (of the ramp-strategy) is zero most of the time, meaning that all the reserves are deployed.

Fig. 10 compares the output power of one of the PV-PPs for a cloudy and sunny day considering the deload strategies under study. The figure confirms that the dynamic control strategies are

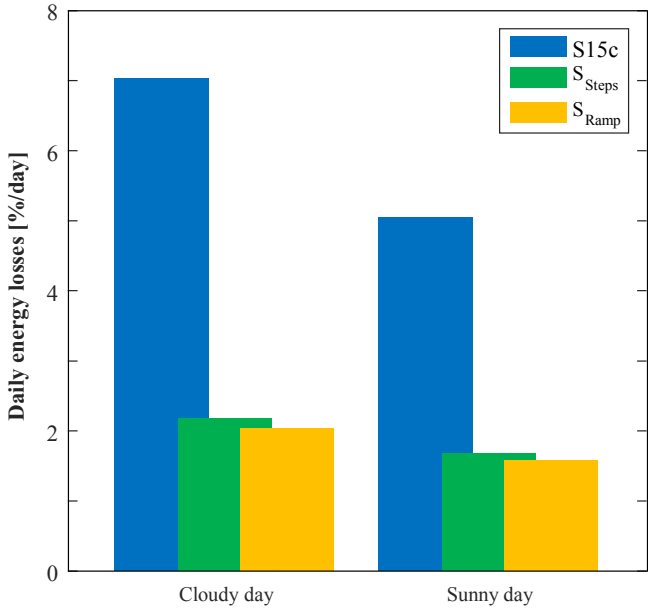

Fig. 8. Total energy losses (for the evaluated days) per control strategy.

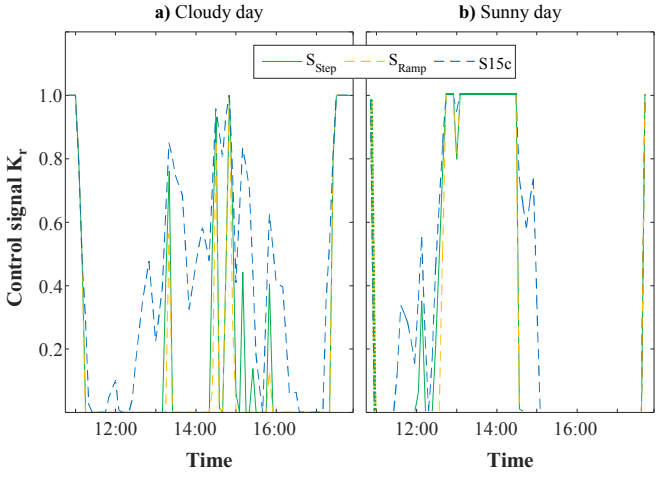

Fig. 9. Control efforts (signal K_r) of the different strategies. a) Cloudy day b) Sunny day.

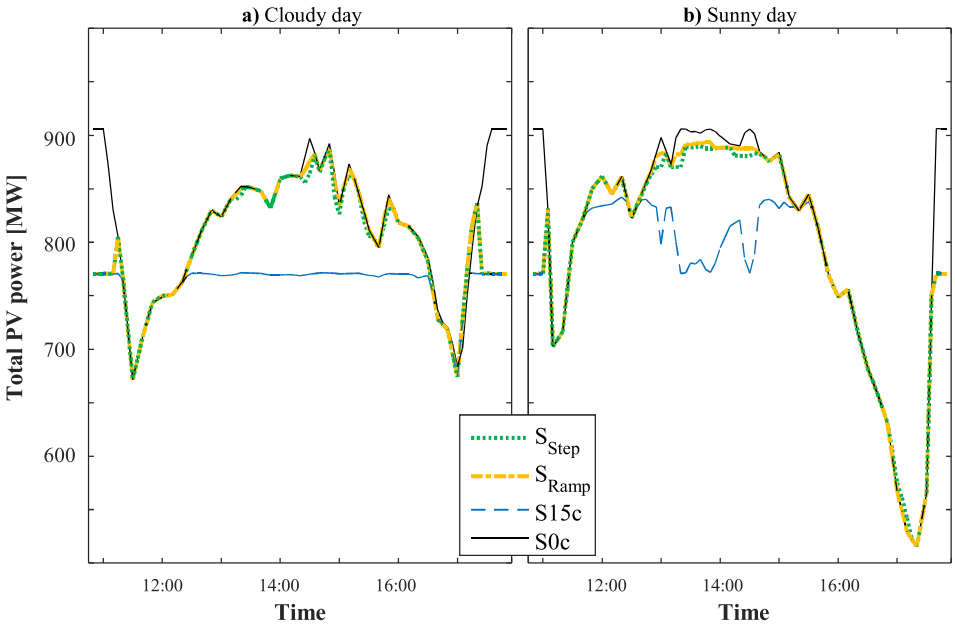

Fig. 10. Output power of a PV-PP for the different deload strategies. a) Cloudy day b) Sunny day.

more efficient, as compared to the case with constant deload level (*S*15*c*), because the energy losses are smaller (the generation profiles of the variable control strategies are closer to the generation profile of the case without deload).

6. Conclusions

This paper proposes a novel control strategy to reduce the impacts that large-scale PV power plants, when operating under partially-shaded conditions, may cause on the frequency regulation of electric power systems. The essence of the controller is to operate different sections of a PV plant in deload mode, allowing the PV modules to keep power reserves. The deload level of each section is dynamically defined during the day considering a 10-min forecast of the solar irradiation.

The proposed forecasting model is based on artificial neural networks, divided into two main stages. The first stage forecasts the type of day based on the clear sky index and the second stage predicts the radiation level. Distinguishing between different types of days shows a better performance (lower errors) than considering only one kind of day. In our case study, the use of three types of days allows for an accurate forecast of irradiation with normalized mean square errors ranging between 1.8% and 2.4%. The results show that to achieve good performance with the artificial neural networks, at least 5 years of measurements are needed.

The dynamic simulations (in DIgSILENT) indicate that the implementation of the proposed control —either with a constant or dynamic deload level strategy— always improves the frequency regulation of the electricity grid. However, from an economic perspective, there is an important difference between considering a constant or dynamic deload level in the PV power plant. Concretely, in our case study, limiting the output power to 85% (15% constant deload level) of the maximum available in the PV power plant implies losing about 7% of energy per day. Instead, a variable deload level achieves energy losses below 2% depending on the kind of day (level of irradiance variability). Accordingly, the PV power plant can operate closer to the maximum power point more often. Thus, a dynamic deload level not only contributes to keeping the frequency of the electricity grid within the allowable band, but also allows decreasing the energy losses, making the implementation of the proposed control economically more attractive.

In view of our results, we proved that our control strategy can efficiently reduce the effects that partially-shaded PV power plants have on the frequency of electricity grids when the deload level is set dynamically during the day. The good performance was achieved not only from a technical viewpoint but also from an economic one. This, in turn, means that to manage electric power systems more economically, the reserve margin kept in PV power plants should vary with time, rather than being fixed for the whole day. These findings give important insights to electricity regulators about how they should define the technical requirements for large-scale PV power plants in grids dominated by solar generation.

As future work, we identify comparing the precision of the artificial neural networks with other forecasting methods that are promising on the pertinent timescale, for example, Markov Chains. Furthermore, understanding the number of critical situations from a power system operation point of view is needed to fully describe the economic impacts of operating the PV power plants in deload mode. In this context, the implementation of our control in PV power plants with energy storage systems may also be an appealing solution in electric power systems with large shares of PV generation. Storage devices can both decrease the energy losses from a deloaded operation and improve the dynamic performance of the electricity grid. We applied a deloaded control strategy as an alternative to potentially more expensive energy storage systems considering current market conditions in Chile. However, the case of other electric power systems with more attractive remuneration schemes for this kind of ancillary service might be different. Regardless of the way in which the control strategy is implemented (by means of deload operation or storage devices), the development of innovative controls, such as the one proposed here, is a key issue to move towards sustainable electrical power systems, while assuring a secure operation of the electricity grid.

Acknowledgment

The authors acknowledge the financial support of the Chilean Council of Scientific and Technological Research, CONICYT/

FONDECYT/11160228, CONICYT/Fondap/15110019, the Complex Engineering Systems Institute (ICM-FIC: P05-004-F, CONICYT: FB0816), and the German Academic Exchange Service.

Annex

Nomenclature of model

Symbol Description

ANNs (Artificial neural networks)

x_{ij}	Signal that neuron i receives from neuron j
w_{i0}	Bias of neuron i
a_i	Internal activity level of neuron i
$\phi(a_i)$	Sigmoid function
y_i	Output of neuron i
CSI_d	Clear sky index of day d
T_d	Temperature of day d
GSR_d	Global radiation of day d

Dynamic control strategy

$\tilde{P}_{out_{t+10}}$	10-min ahead forecast of solar power
P_{out_t}	Current solar power
χ	Deload level of the power plant
K_r	Control signal to alter the deload level as a function of operating conditions
H	Solar radiation (in the corresponding time step)
T	Cell temperature (in the corresponding time step)
$P^i_{mpp}(H,T)$	Maximum power output of section i as a function of H and T
$R_t(\chi)$	Amount of available operating reserves in the power plant
ΔP	Power deficit caused by partial shading

References

Ahrens, C., 2012. Meteorology Today: an Introduction to Weather, Climate, and the Environment, tenth ed. Brooks/Cole, CENGAGE Learning, Belmont, CA.

Bacher, P., Madsen, H., Nielsen, H.A., 2009. Online short-term solar power forecasting. Sol. Energy 83, 1772–1783. https://doi.org/10.1016/j.solener.2009.05.016.

Beltran, H., Bilbao, E., Belenguer, E., Etxeberria-Otadui, I., Rodriguez, P., 2013. Evaluation of storage energy requirements for constant production in PV power plants. IEEE Trans. Ind. Electron. 60, 1225–1234. https://doi.org/10.1109/TIE.2012.2202353.

Bhandari, R., Trudewind, C.A., Zapp, P., 2014. Life cycle assessment of hydrogen production via electrolysis - a review. J. Clean. Prod. 85, 151–163. https://doi.org/10.1016/j.jclepro.2013.07.048.

Bidram, A., Davoudi, A., Balog, R.S., 2012. Control and circuit techniques to mitigate partial shading effects in photovoltaic arrays. IEEE J. Photovoltaics 2, 532–546. https://doi.org/10.1109/JPHOTOV.2012.2202879.

Box, G., Jenkins, G., Reinsel, G., Ljung, G., 2015. Time Series Analysis: Forecasting and Control.

Carvalho, P.M.S., Ferreira, L. a F.M., Krogh, B.H., Popli, N., Ilic, M.D., 2011. Wind integration in power systems: operational challenges and possible solutions. Proc. IEEE 99, 214–232. In: https://doi.org/10.1109/JPROC.2010.2070051.

Cebulla, F., Haas, J., Eichman, J., Nowak, W., Mancarella, P., 2018. How much electrical energy storage do we need? A synthesis for the U.S., Europe, and Germany. J. Clean. Prod. 181, 449–459. https://doi.org/10.1016/j.jclepro.2018.01.144.

Centro de Energía - University of Chile, 2018. Complementary Data of Publications [WWW Document]. URL. http://centroenergia.cl/Docs/ (accessed 7.16.18).

Chen, C., Duan, S., Cai, T., Liu, B., 2011. Online 24-h solar power forecasting based on weather type classification using artificial neural network. Sol. Energy 85, 2856–2870. https://doi.org/10.1016/j.solener.2011.08.027.

Chow, C.W., Urquhart, B., Lave, M., Dominguez, A., Kleissl, J., Shields, J., Washom, B., 2011. Intra-hour forecasting with a total sky imager at the UC San Diego solar energy testbed. Sol. Energy 85, 2881–2893. https://doi.org/10.1016/j.solener.2011.08.025.

Cordero, R.R., Damiani, A., Seckmeyer, G., Jorquera, J., Caballero, M., Rowe, P., Ferrer, J., Mubarak, R., Carrasco, J., Rondanelli, R., Matus, M., Laroze, D., 2016. The solar spectrum in the Atacama desert. Sci. Rep. 6, 22457. https://doi.org/10.1038/srep22457.

Craciun, B.-I., Spataru, S., Kerekes, T., Sera, D., Teodorescu, R., 2013. Power ramp limitation and frequency support in large scale PVPPs without storage. In: 2013 IEEE 39th Photovoltaic Specialists Conference (PVSC). IEEE, pp. 2354–2359. https://doi.org/10.1109/PVSC.2013.6744947.

Department of Geophysics - University of Chile, Ministry of Energy of Chile, 2012. Explorador de energía solar (Solar energy explorer) [WWW Document]. URL. http://walker.dgf.uchile.cl/Explorador/Solar2/ (accessed 8.25.15).

Diagne, M., David, M., Lauret, P., Boland, J., Schmutz, N., 2013. Review of solar irradiance forecasting methods and a proposition for small-scale insular grids. Renew. Sustain. Energy Rev. 27, 65–76. https://doi.org/10.1016/j.rser.2013.06.042.

Duchaud, J.-L., Notton, G., Darras, C., Voyant, C., 2018. Power ramp-rate control algorithm with optimal state of charge reference via dynamic programming. Energy 149, 709–717. https://doi.org/10.1016/J.ENERGY.2018.02.064.

El-Dein, M.Z.S., Kazerani, M., Salama, M.M.A., 2011. Novel configurations for photovoltaic farms to reduce partial shading losses. In: 2011 IEEE Power and Energy Society General Meeting. IEEE, pp. 1–5. https://doi.org/10.1109/PES.2011.6039636.

Eto, J., Undrill, J., Mackin, P., Daschmans, R., Williams, B., Haney, B., Hunt, R., Ellis, J., Illian, H., Martinez, C., ÓMalley, M., Coughlin, K., Hamachi-LaCommare, K., 2010. Use of Frequency Response Metrics to Assess the Planning and Operating Requirements for Reliable Integration of Variable Renewable Generation. Lawrence Berkeley National Laboratory, Berkeley, CA, USA. Rep. LBNL-4142E.

Faranda, R., Leva, S., 2008. Energy comparison of MPPT techniques for PV systems. WSEAS Trans. Power Syst. 3, 446–455.

Guishi Wang, Ciobotaru, M., Agelidis, V.G., 2012. Minimising output power fluctuation of large photovoltaic plant using vanadium redox battery storage. In: 6th IET International Conference on Power Electronics, Machines and Drives (PEMD 2012). IET. D41–D41. https://doi.org/10.1049/cp.2012.0331.

Haas, J., Palma-Behnke, R., Valencia, F., Araya, P., Díaz-Ferrán, G., Telsnig, T., Eltrop, L., Díaz, M., Püschel, S., Grandel, M., Román, R., Jiménez-Estévez, G., 2018. Sunset or sunrise? Understanding the barriers and options for the massive deployment of solar technologies in Chile. Energy Pol. 112, 399–414. https://doi.org/10.1016/j.enpol.2017.10.001.

Harvey, A., 1990. Forecasting, Structural Time Series Models and the Kalman Filter.

Hašková, S., 2017. Holistic assessment and ethical disputation on a new trend in solid biofuels. Sci. Eng. Ethics 23, 509–519. https://doi.org/10.1007/s11948-016-9790-1.

Hernández, J.C., Bueno, P.G., Sanchez-Sutil, F., 2017. Enhanced utility-scale photovoltaic units with frequency support functions and dynamic grid support for transmission systems. IET Renew. Power Gener. 11, 361–372. https://doi.org/10.1049/iet-rpg.2016.0714.

Hill, C. a., Such, M.C., Chen, D., Gonzalez, J., Grady, W.M., 2012. Battery energy storage for enabling integration of distributed solar power generation. IEEE Trans. Smart Grid 3, 850–857. https://doi.org/10.1109/TSG.2012.2190113.

Hoff, T.E., Perez, R., 2010. Quantifying PV power output variability. Sol. Energy 84, 1782–1793. https://doi.org/10.1016/j.solener.2010.07.003.

Huang, J., Korolkiewicz, M., Agrawal, M., Boland, J., 2013. Forecasting solar radiation on an hourly time scale using a Coupled AutoRegressive and Dynamical System (CARDS) model. Sol. Energy 87, 136–149. https://doi.org/10.1016/j.solener.2012.10.012.

Inman, R.H., Pedro, H.T.C., Coimbra, C.F.M., 2013. Solar forecasting methods for renewable energy integration. Prog. Energy Combust. Sci. 39, 535–576. https://doi.org/10.1016/J.PECS.2013.06.002.

Ishaque, K., Salam, Z., Amjad, M., Mekhilef, S., 2012. An improved particle swarm optimization (PSO)-based MPPT for PV with reduced steady-state oscillation. IEEE Trans. Power Electron. 27, 3627–3638. https://doi.org/10.1109/TPEL.2012.2185713.

Jones, L., 2017. Renewable Energy Integration: Practical Management of Variability, Uncertainty, and Flexibility in Power Grids. Academic Press.

Jurasz, J., Ciapała, B., 2017. Integrating photovoltaics into energy systems by using a run-off-river power plant with pondage to smooth energy exchange with the power gird. Appl. Energy 198, 21–35. https://doi.org/10.1016/J.APENERGY.2017.04.042.

Kakimoto, N., Satoh, H., Takayama, S., Nakamura, K., 2009. Ramp-rate control of photovoltaic generator with electric double-layer capacitor. IEEE Trans. Energy Convers. 24, 465–473. https://doi.org/10.1109/TEC.2008.2001580.

Kankiewicz, A., Moon, D., Sengupta, M., 2010. Observed impacts of transient clouds on utility-scale PV fields. In: ASES National Solar Conference, pp. 1–4.

Kouro, S., Leon, J.I., Vinnikov, D., Franquelo, L.G., 2015. Grid-connected photovoltaic systems: an overview of recent research and emerging PV converter technology. Ind. Electron. Mag. IEEE 9, 47–61. https://doi.org/10.1109/MIE.2014.2376976.

Larrañeta, M., Moreno-Tejera, S., Silva-Pérez, M.A., Lillo-Bravo, I., 2015. An improved model for the synthetic generation of high temporal resolution direct normal irradiation time series. Sol. Energy 122, 517–528. https://doi.org/10.1016/j.solener.2015.09.030.

Lave, M., Kleissl, J., 2013. Cloud speed impact on solar variability scaling - application to the wavelet variability model. Sol. Energy 91, 11–21. https://doi.org/10.1016/j.solener.2013.01.023.

Lew, D., Brinkman, G., Kumar, N., Lefton, S., Jordan, G., Venkataraman, S., 2013. Finding flexibility: cycling the conventional fleet. IEEE Power Energy Mag. 11, 20–32. https://doi.org/10.1109/MPE.2013.2277988.

Li, Q., Wolfs, P., 2008. A review of the single phase photovoltaic module integrated converter topologies with three different DC link configurations. IEEE Trans. Power Electron. 23, 1320–1333. https://doi.org/10.1109/TPEL.2008.920883.

Liu, J., Fang, W., Zhang, X., Yang, C., 2015. An improved photovoltaic power forecasting model with the assistance of aerosol index data. IEEE Trans. Sustain. Energy 6, 434–442. https://doi.org/10.1109/TSTE.2014.2381224.

Mäki, A., Valkealahti, S., 2012. Power losses in long string and parallel-connected short strings of series-connected silicon-based photovoltaic modules due to partial shading conditions. IEEE Trans. Energy Convers. 27, 173–183. https://doi.org/10.1109/TEC.2011.2175928.

Mao, M., Gong, W., Chang, L., 2013. Short-term photovoltaic output forecasting model for economic dispatch of power system incorporating large-scale photovoltaic plant. In: 2013 IEEE Energy Conversion Congress and Exposition, ECCE 2013, pp. 4540–4545. https://doi.org/10.1109/ECCE.2013.6647308.

Mardoyan, A., Braun, P., 2015. Analysis of Czech subsidies for solid biofuels. Int. J. Green Energy 12, 405–408. https://doi.org/10.1080/15435075.2013.841163.

Maroušek, J., Itoh, S., Higa, O., Kondo, Y., Ueno, M., Suwa, R., Tominaga, J., Kawamitsu, Y., 2013. Enzymatic hydrolysis enhanced by pressure shockwaves opening new possibilities in Jatropha Curcas L. processing. J. Chem. Technol. Biotechnol. 88, 1650–1653. https://doi.org/10.1002/jctb.4014.

McLellan, B.C., Corder, G.D., Giurco, D.P., Ishihara, K.N., 2012. Renewable energy in the minerals industry: a review of global potential. J. Clean. Prod. 32, 32–44. https://doi.org/10.1016/j.jclepro.2012.03.016.

Mills, A.D., Wiser, R.H., 2011. Implications of geographic diversity for short-term variability and predictability of solar power. In: 2011 IEEE Power and Energy Society General Meeting. IEEE, pp. 1–9. https://doi.org/10.1109/PES.2011.6039888.

Mills, A., Ahlstrom, M., Brower, M., Ellis, A., George, R., Hoff, T., Kroposki, B., Lenox, C., Miller, N., Milligan, M., Stein, J., Wan, Y., 2010. Understanding Variability and Uncertainty of Photovoltaics for Integration with the Electric Power System. Lawrence Berkeley National Laboratory. Lawrence Berkeley National Laboratory, Berkeley, CA, USA. Rep. LBNL-2855E. https://doi.org/10.1109/MPE.2011.940575.

Moreno-Leiva, S., Díaz-Ferrán, G., Haas, J., Telsnig, T., Díaz-Alvarado, F. a., Palma-Behnke, R., Kracht, W., Román, R., Chudinzow, D., Eltrop, L., 2017. Towards solar power supply for copper production in Chile: assessment of global warming potential using a life-cycle approach. J. Clean. Prod. 164, 242–249. https://doi.org/10.1016/j.jclepro.2017.06.038.

National Commission of Energy, 2016. Norma Técnica de Seguridad y Calidad de Servicio (Technical norm for power security and quality).

National Energy Commission of Chile (CNE), 2016. Informe Preliminar de Previsión de Demanda 2016-2036, SIC-SING (Report on the demand projection for 2016-2036 in Central and Northern Chile). Santiago, Chile.

National Energy Commission of Chile (CNE), 2017. Statistics of Electricity [WWW Document]. URL. https://www.cne.cl/wp-content/uploads/2015/05/Capacidad_Instalada_Generación.xlsx (accessed 4.20.17).

Ngoko, B.O., Sugihara, H., Funaki, T., 2014. Synthetic generation of high temporal resolution solar radiation data using Markov models. Sol. Energy 103, 160–170. https://doi.org/10.1016/j.solener.2014.02.026.

Pamparana, G., Kracht, W., Haas, J., Díaz-Ferrán, G., Palma-Behnke, R., Román, R., 2017. Integrating photovoltaic solar energy and a battery energy storage system to operate a semi-autogenous grinding mill. J. Clean. Prod. 165, 273–280. https://doi.org/10.1016/j.jclepro.2017.07.110.

Papaefthymiou, G., Schavemaker, P.H., van der Sluis, L., Kling, W.L., Kurowicka, D., Cooke, R.M., 2006. Integration of stochastic generation in power systems. Int. J. Electr. Power Energy Syst. 28, 655–667. https://doi.org/10.1016/j.ijepes.2006.03.004.

Pelland, S., Remund, J., Kleissl, J., Oozeki, T., Brabandere, K. De, 2013. Photovoltaic and Solar Forecasting: State of the Art, International Energy Agency: Photovoltaic Power Systems Programme. Report IEA PVPS T14. https://doi.org/978-3-906042-13-8.

Rahmann, C., Vittal, V., Ascui, J., Haas, J., 2016. Mitigation control against partial shading effects in large-scale PV power plants. IEEE Trans. Sustain. Energy 7, 173–180. https://doi.org/10.1109/TSTE.2015.2484261.

Rani, B.I., Ilango, G.S., Nagamani, C., 2013. Enhanced power generation from PV array under partial shading conditions by shade dispersion using Su Do Ku configuration. IEEE Trans. Sustain. Energy 4, 594–601. https://doi.org/10.1109/TSTE.2012.2230033.

Rehman, S., Mohandes, M., 2008. Artificial neural network estimation of global solar radiation using air temperature and relative humidity. Energy Pol. 36, 571–576. https://doi.org/10.1016/j.enpol.2007.09.033.

Reikard, G., 2009. Predicting solar radiation at high resolutions: a comparison of time series forecasts. Sol. Energy 83, 342–349. https://doi.org/10.1016/j.solener.2008.08.007.

Remund, J., Calhau, C., Perret, L., Marcel, D., 2015. Characterization of the spatio-temporal variations and ramp rates of solar radiation and PV. In: IEA PVPS T14-05:2015.

REN21, 2017. Renewables 2017-Global Status Report. Paris, France.

Rigollier, C., Lefèvre, M., Wald, L., 2004. The method Heliosat-2 for deriving shortwave solar radiation from satellite images. Sol. Energy 77, 159–169. https://doi.org/10.1016/j.solener.2004.04.017.

Ruiz-Rodriguez, F.J., Bueno, P.G., Hernández, J.C., 2016. Stability assessment for transmission systems with large utility-scale photovoltaic units. IET Renew. Power Gener. 10, 584–597. https://doi.org/10.1049/iet-rpg.2015.0331.

Shi, J., Lee, W.J., Liu, Y., Yang, Y., Wang, P., 2012. Forecasting power output of photovoltaic systems based on weather classification and support vector machines. In: IEEE Transactions on Industry Applications, pp. 1064–1069. https://doi.org/10.1109/TIA.2012.2190816.

Shivashankar, S., Mekhilef, S., Mokhlis, H., Karimi, M., 2016. Mitigating methods of power fluctuation of photovoltaic (PV) sources – a review. Renew. Sustain. Energy Rev. 59, 1170–1184. https://doi.org/10.1016/j.rser.2016.01.059.

Solargis s.r.o, 2018. Solargis: IMaps [WWW Document]. URL. https://solargis.info/imaps/ (accessed 5.22.18).

SolarPower Europe, 2017. Global Market Outlook - for Solar Power 2017-2021. SolarPower Europe, Brussels.

Tey, Kok Soon, Mekhilef, S., 2014. Modified incremental conductance algorithm for photovoltaic system under partial shading conditions and load variation. IEEE Trans. Ind. Electron. 61, 5384–5392. https://doi.org/10.1109/TIE.2014.2304921.

Voyant, C., Notton, G., Kalogirou, S., Nivet, M.-L., Paoli, C., Motte, F., Fouilloy, A., 2017. Machine learning methods for solar radiation forecasting: a review. Renew. Energy 105, 569–582. https://doi.org/10.1016/J.RENENE.2016.12.095.

Xin, H., Liu, Y., Wang, Z., Gan, D., Yang, T., 2013. A new frequency regulation strategy for photovoltaic systems without energy storage. IEEE Trans. Sustain. Energy 4, 985–993. https://doi.org/10.1109/TSTE.2013.2261567.

Yang, Y., Blaabjerg, F., Wang, H., 2014. Constant power generation of photovoltaic systems considering the distributed grid capacity. In: 2014 IEEE Applied Power Electronics Conference and Exposition - APEC 2014. IEEE, pp. 379–385. https://doi.org/10.1109/APEC.2014.6803336.

Zhang, Y., Beaudin, M., Zareipour, H., Wood, D., 2014. Forecasting Solar Photovoltaic power production at the aggregated system level. In: 2014 North American Power Symposium (NAPS). IEEE, pp. 1–6. https://doi.org/10.1109/NAPS.2014.6965389.